文章编号：1001－9014(2018)02－0177－07

DOI:10.11972/j.issn.1001－9014.2018.02.009

PolSAR image classification based on sparse autoencoder and boundary-preserved WMRF

ZHANG Shu-Yin, HOU Biao*, JIAO Li-Cheng, WU Qian

(Key Laboratory of Intelligent Perception and Image Understanding of Ministry of Education, International Research Center of Intelligent Perception and Computation, International Collaboration Joint Lab in Intelligent Perception and Computation, Xidian University, Xi'an 710071, China)

Abstract: In order to solve problem of the limited training samples and keep consistency in one region, a new two-level classification scheme is proposed, which combines sparse auto-encoder (SAE) and Boundary-preserved Wishart-markov random fields (BWMRF). In the first layer, an SAE classifier is applied to obtain an initial classification and more accurate regional boundaries. In the second layer, Boundary-preserved Wishart-markov random fields have been used to correct the previous classification results. Meanwhile, the boundaries classified by sparse auto-encoder are preserved, and a new error correction strategy is applied to ensure the classification accuracy. Therefore, accurate region boundaries supplied by SAE are explored to divide different regions, and the coherent in each region will be realized during the BWMRF process. Compared with other classification methods, this method obtains higher classification accuracy and proves the validity of the new scheme.

Key words: sparse auto-encoder (SAE), polarimetric synthetic aperture radar (PolSAR) images, Wishart distance, Markov random fields (MRF)

PACS: 29.25.Pj, 84.40.Xb

基于稀疏自编码器和边缘保持的 Wishart 马尔科夫随机场的极化 SAR 图像分类

张姝茵, 侯 彪*, 焦李成, 吴 倩

(西安电子科技大学 智能感知与图像理解教育部重点实验室、智能感知与计算国际联合研究中心、智能感知与计算国际合作联合实验室, 陕西 西安 710071)

摘要:针对极化SAR图像训练样本数目较少问题以及极化SAR图像同质区域较多的特性,提出了一种新的两层分类框架,结合了稀疏自编码器和边缘保持的Wishart马尔科夫随机场对极化SAR图像进行分类.该框架包括个步骤,第一个步骤使用稀疏自编码器来获得一个初始分类;第二个步骤使用边缘保持的Wishart马尔科夫随机场对第一层的分类结果进行修正.在应用Wishart马尔科夫随机场的过程中,由稀疏自编码器分类得到的边缘得以保持,并且提出了新的分类错误纠正策略确保分类的准确性.因此,通过稀疏自编码器得到的精确分类边缘可用于不同的区域并且在应用Wishart马尔科夫的过程中得以保持.和其他分类方法相比,该方法得到较高的分类精度,证明了新方法的有效性.

关 键 词:稀疏自编码器;极化SAR图像;Wishart距离;马尔科夫随机场

中图分类号:TP751.1 **文献标识码**:A

Received date: 2017-07-05, **revised date**: 2017-12-20 **收稿日期**:2017-07-05, **修回日期**:2017-12-20

Foundation items: Supported by National Natural Science Foundation of China (61671350, 61573267, 61473215, 61572383, 61502369), and the National Basic Research Program (973 Program) of China (2013CB329402)

Biography: ZHANG Shu-Yin (1982-), female, Xi'an, China, Ph. D. Research area involves PolSAR image interpretation and processing. E-mail: zhangsy217@163.com

* **Corresponding author**: E-mail: avcodec@163.com

Introduction

Synthetic aperture radar (SAR) image processing is one of the most important applications in geoscience and remote sensing[1-2]. PolSAR records the target backscattering information completely by measuring each unit in different polarization channels, which has been applied widely in many fields such as agriculture, geology and military in the last two decades[3-5]. With the fact that more than one polarization is used, much richer characterization of the observed land-cover types and other targets are obtained. However, the complexity of the data requires increasing analysis and interpretation.

The land cover classification of PolSAR data is a powerful and important application in remote sensing image field, where each pixel of the data is assigned to a certain class. In recent years, many methods have been developed[6-8] for PolSAR image classification, among which machine learning is found to be highly effective and commonly used in the application of SAR image[9-11]. However, these traditional algorithms cannot learn hierarchical representations of the objects with discriminative information. Since 2006, machine learning has made breakthroughs. Hinton et. al. proposed the concept of deep learning for the first time which is similar to the multilayer physical structure of the human learning system[12]. Deep learning methods can automatically extract features from the data with multiple layers. In the remote sensing field, deep learning algorithm is implemented to solve image classification problems successfully[13]. Wang et. al designed a classification framework with deep convolutional neural network (CNN) for PolSAR image[14]. They made use of CNNs to extract and learn rich features from the training data. Xie *et al.* proposed Wishart autoencoder (WAE) and Wishart convolutional autoencoder (WCAE) for PolSAR image classification[15]. In the proposed method, the Wishart distance measurement is combined into the training process of the AE and the CAE. A classification method with local deep spatial sparse feature is proposed by Zhang et al. [16] In this paper, the local spatial information is introduced into stacked sparse autoencoder (SSAE) to learn the deep spatial sparse features automatically.

It appears clearly from the above works that deep learning is becoming very attractive for PolSAR image processing. We propose to address the issues of PolSAR classification with a usual model sparse SAE[17]. In many problems, a large number of training samples lead to data diversity and robust features. However, the limited number of labeled training samples becomes a critical problem for PolSAR data. As one of the excellent methods, SAE can automatically learn useful features layer-by-layer in an unsupervised manner and very few training samples are used for fine-tuning. In this way, the method needs little initial labeled data. Therefore, SAE is utilized to extract the feature in our classification framework. Nonetheless, SAE is a pixel-based method. In other words, the label is assigned pixel by pixel in SAE. Hence, it will be benefit to obtain accurate boundary of the object.

Nevertheless, the influence of speckle cannot be avoided and it yields a discontinuous classification result by SAE. In the PolSAR terrain classification, there are a lot of small regions within one object. Hence, Wishatmarkov random fields (WMRF) algorithm has been used to smooth the region and alleviate the uncertainty and fuzziness[18]. The traditional WMRF often consists of two stages: an initial over-segmentation and final classification. First, an image is over-segmented into a large amount of rectangular regions. As a result, the pixels near the boundaries can be included into the same rectangular regions. Hence, these pixels are often misclassified. Second, each region should be assigned an appropriate label. In this way, some pixels are forced into a certain category. To solve these problems, a boundary-preserved WMRF (BWMRF) with an error correct strategy is proposed to preserve the boundaries got from SAE. In order to obtain the accurate boundaries and homogenous regions simultaneously, the combination of SAE and BWMRF is proposed in our strategy.

There are several advantages of the proposed model. The main novel contributions of this paper are:

First, a novel two-layer classification scheme is proposed. The first layer shows an initial classification and provides abundant information to improve the boundary result by SAE. Due to the label is assigned pixel by pixel, SAE has more accurate region boundaries. The second layer is designed based on the spatial information of PolSAR data to revise the probability by BWMRF.

Second, in order to explore the spatial information of the image, BWMRF is proposed. In the BRMRF process, the boundary-preserve and error correction strategies are proposed to supply smoother classification map and preserve the boundary adaptively.

The remainder of this paper is organized as follows. Section 1 presents a brief presentation of back ground. In Sect. 2, the proposed method is discussed in detail. Experiments and discussions are given in Sect. 3. Section 4 presents the conclusions.

1 Brief overview on PolSAR image, SAE and WMRF

1.1 Polarimetric SAR image

For the monostatic case with a reciprocal medium, the complex scattering vector is

$$\boldsymbol{h} = [S_{HH} \quad \sqrt{2}S_{HV} \quad S_{VV}]^{\mathrm{T}} \quad , \quad (1)$$

where the superscript T denotes the matrix transpose[19].

Multi-look processing is often performed for speckle reduction and the polarimetric covariance matrix can be represented as follows:

$$\boldsymbol{C} = \frac{1}{N}\sum_{i=1}^{N} h_i h_i^{*\mathrm{T}} = \begin{bmatrix} C_{11} & C_{12} & C_{13} \\ C_{21} & C_{22} & C_{23} \\ C_{31} & C_{32} & C_{33} \end{bmatrix}^{\mathrm{T}} \quad , \quad (2)$$

where $\boldsymbol{h}_i$ denotes the ith single-look scattering vector, N is the number of looks and the superscript $*$ denotes the complex conjugate.

1.2 Sparse autoencoder

As an unsupervised method to learn the feature from the unlabeled data, autoencoder (AE) is composed of an encoder and a decoder. It is trained to minimize the reconstruction error between the input in the encoding layer

and the output in the decoding layer. SAE is the method which adds the restricted condition of sparse representation into AE during encoding process[20]. The structure is shown in Fig. 1.

Suppose the input data $x_i \in R^n$ and $a_i \in R^m$, (the superscript is the dimension of the input data, i is the index of the ith data, and is the dimension of the hidden layer nodes) then the encoder can be represented as:

$$a_i = f(W^{(1)}x_i + b^{(1)}) \quad , \quad (3)$$

where $W^{(1)} \in R^{m\times n}$ is the weight matrix between the input layer and hidden layer, f is a nonlinear activation function hidden layer, a logistic sigmoid function is applied here: $f(z) = 1/(1+\exp(-z))$ and $b^{(1)} \in R^{m\times 1}$ is the bias vector of the hidden layer.

To obtain the reconstruction value, the decoder is used. It maps the latent representation $a_(i) \in R^m$ to a reconstruction. It can be expressed as:

$$y_i = g(W^{(2)}a_i + b^{(2)}) \quad , \quad (4)$$

where $W^{(2)} \in R^{n\times m}$ is the weight matrix between the hidden layer and the output layer, $b^{(2)} \in R^{n\times 1}$ is the bias vector of the output layer and the activation function of output unit with the logistic sigmoid form is $g(z) = z$.

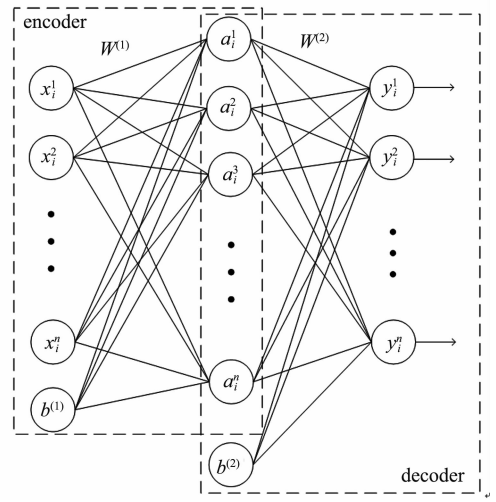

Fig. 1　The structure of SAE
图 1　SAE 结构

The aim of the training process is to recover the input data. In the other words, the output $\boldsymbol{y}$ should be as close as possible to the input $\boldsymbol{x}$. The minimum value of cost function is got by back propagation training. It can be written as a mean squared-error function:

$$J = \frac{1}{2M}\sum_{i=1}^{M}\|y_i - x_i\|^2 \quad , \quad (5)$$

where M is the number of input data.

When the autoencoder has more hidden units than inputs, we can obtain a good representation, which is a overcomplete problem. Moreover, the expected activation of the hidden units is constrained to be sparse. Then the cost function is written as:

$$J_{\text{sparse}} = \frac{1}{2M}\sum_{i=1}^{M}\|y_i - x_i\|^2 + \lambda\sum_{j=1}^{m}KL(\rho\|\hat{\rho}_j) \quad , \quad (6)$$

where λ controls the weight of the sparsity penalty term, $\mathrm{KL}(\rho\|\hat{\rho}_j)$ is the relative entropy:

$$(\rho\|\hat{\rho}_j) = \rho\log\frac{\rho}{\hat{\rho}_j} + (1-\rho)\log\frac{1-\rho}{1-\hat{\rho}_j} \quad , \quad (7)$$

where ρ is the sparse parameter, $\hat{\rho}_j$ is the average activation of hidden unit.

1.3　Wishart Markov random fields

MRF model is widely used in image processing because it can make full use of the contextual information[18].

If there is an image with the size of $M \times N$, we can regard the image as a number set on a 2-D lattice $S = \{s_{ij}, 1 \leqslant i \leqslant M, 1 \leqslant j \leqslant N\}$, where s_{ij} locates in (i,j). The essence of classification is to estimate class label for each pixel. Set $X = \{x_s, s \in S\}$ be an observed image and $Y = \{y_s, s \in S\}$ are the class labels of X. The random field Y is Markov random fields that can be describe as

$$P(y_s \mid y_{\eta_s}) = \frac{\exp\{-U(y_s)\}}{\sum_{y_s=1}^{K}\exp\{-U(y_s)\}} = \frac{\exp\{\beta u(y_s)\}}{\sum_{y_s=1}^{K}\exp\{\beta u(y_s)\}} \quad , \quad (8)$$

where $\beta > 0$ is the spatial smoothness parameter, $u(y_s) = \sum_{t\in\eta_s}\delta(y_s - y_t)$ is the number of pixels, and y_t are the labels of the pixels in the neighbor η_s.

The label of pixel s can be computed by:

$$y_s = \arg\max_{y\in\{1,\cdots,K\}}\{p(x_s \mid y_s)P(y_s \mid y_{\eta_s})\} \quad , \quad (9)$$

where $p(x_s \mid l_s)$ is the conditional probability of the observed data.

In the traditional PolSAR data processing, Wishart distribution can describe the statistical property of the PolSAR data very well. The Wishart MRF model can be defined as:

$$P(y_s \mid x_s) = \frac{L^{qL}\mid C_s\mid^{L-q}\exp\{\beta\mu(y_s) - LTr(\sum_a^{-1}C_s)\}}{R(L,q)\mid\sum_a\mid^L\sum_{y_s=1}^{k}\exp\{\beta\mu(y_s)\}} \quad . \quad (10)$$

Then the label of pixel s becomes:

$$\hat{y}_s = \arg\max_{y_s\in\{1\cdots K\}} = \frac{L^{qL}\mid C_s\mid^{L-q}\exp\{\beta\mu(y_s) - LTr(\sum_a^{-1}C_s)\}}{R(L,q)\mid\sum_a\mid^L\sum_{y_s=1}^{k}\exp\{\beta\mu(y_s)\}} \quad . \quad (11)$$

2　The proposed method for PolSAR image classification

In this article, a new method which combines SAE and BWMRF classification for PolSAR image is proposed, SABM for short. The framework can be regard as a two-layer neural network. The first layer gives an output with the accurate region boundaries of classification. Then, the second layer is constructed to revise the probability of the output of the first layer and the boundaries supplied by the first layer are remained during the process. The flow chart is as follows.

The implementation procedure of the proposed method includes two layers:

layer 1: The SAE has been applied in layer 1. So

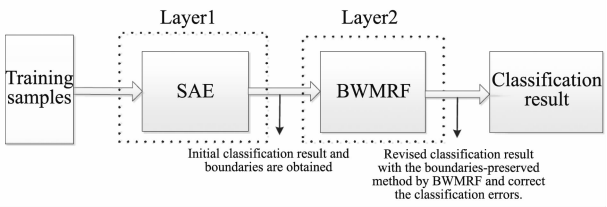

Fig. 2 The flow chart of SABM
图 2 SABM 流程图

we get an initial classification result and classification boundaries.

layer 2: There are some misclassifications of pixels after the first layer, so BWMRF was used to revise the probability to get the correct classification for each pixel. At the same time, the edge was remained during the procedure.

There are two key problems in the proposed method. How to preserve the boundaries and how to correct the classification error during the WMRF used.

(a) Boundary-preserved WMRF

To get more accurate classification result and to alleviate the spatial heterogeneity problem, the segmentation is used before BWMRF. The segmentation operation in the article is divided into two steps.

Step1: We can get an initial classification result from SAE. In order to get the boundary of the classification result, the region of classification map is marked as binary images. Then we can get a rough segmentation map.

Step2: The region is divided after the last step. However, there are some small blocks that were classified by mistake in the regions. To correct the misclassification of the small block, the algorithm with a 4-neighborhood was used. The small blocks are deleted.

After the two steps, we can get a result with the region edges of classification. But the information of the region still has not been considered and there are also many pixels classified by mistake in the regions. In order to exploit the spatial information to refine the classification results, WMRF is used. WMRF make good use of spatial information as a probabilistic model and it can use integrated spatial contextual information into image classification problems. However, during the process of WMRF, the pixels near the boundaries were often regarded as the same category. So the Boundary-Preserved MRF is proposed. The boundaries are got from SAE by step1. The location where the label value changes can be regarded as an edge. In this model, boundaries which got from segmentation process are remained. Therefore, the more accurate classification result can be got. The initial classification map with the boundaries is got after the segmentation. In order to remain the boundaries and to get the coherent region, the regions of the map are divided into smaller regions. Then WMRF is applied to revise the classification result which got from SAE. At the same time, the boundaries are remained.

(b) Error correct for Boundary-preserved WMRF

We can get satisfied results after BWMRF. However, there are some pixels misclassified by WMRF process. There are two steps in WMRF. The first step is segmentation, where the image can be segmented to several blocks. The second step is smoothness. The pixels are replaced by the class which has the maximum number of labels in a block. In this case, some pixels were misclassified.

In order to alleviate this problem, an error correct method is proposed. We can get a confusion matrix when the training of SAE has completed. Columns of confusion matrix represent the number of predicted labels and the rows are the true labels.

The error correcting achieves by the following step. First, calculate the confusion matrix $\boldsymbol{C}_{\text{con}}$ and transform it into the probability form $\boldsymbol{C}_{\text{pro}}$. The elements in $\boldsymbol{C}_{\text{pro}}$ can be calculated by Eq. (12)

$$P(y=l \mid y=i)=\frac{N_{\text{um}}(C_{\text{con}}(i,l))}{\sum_{l} N_{\text{um}}(C_{\text{con}}(i,l))}, \quad (12)$$

where $P(y=l \mid y=i)$ is the probability that if the pixel belongs to categoryotherwise is classified into *lth* category, $N_{\text{um}}(C_{\text{con}}(i,l))$ is the number of labels which represents category i and classified into category l, $\sum_{l} N_{\text{um}}(C_{\text{con}}(i,l))$ is the total number of l-th class.

Second, set a threshold value κ which obtains from $\boldsymbol{C}_{\text{pro}}$. The threshold value is selected by the following procedure. The elements of $\boldsymbol{C}_{\text{pro}}$ are sorted in ascending order. Then average the top 10 percent of data. The result can be saved as threshold value κ. If the value of element in $\boldsymbol{C}_{\text{pro}}$ is less than κ, the elements are regarded as 0. That is to say, if the probability that categoryclassified into categoryless than κ, the probability is set to 0.

Finally, the label is remained when WMRF applied.

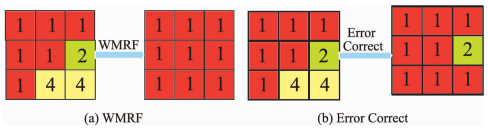

Fig. 3 (a) WMRF, (b) Error Correct
图 3 (a) WMRF, (b) 错误纠正

Figure 3 shows the process of WMRF and error correct, respectively. In traditional WMRF, if the number of categoryis the most, the labels of the whole block are considered as category . The error correct process is exhibited in Fig. 3(b). If the probability that category classified into category is very small, then category is remained during the WMRF process.

3 Experiments and discussions

There are two datasets used in our experience. The first one is Flevoland with the size of 270 × 300, acquired by the AIRSAR platform on 495 August 16, 1989, as shown in Fig. 3(a). It is a four-look polarimetric L-band scene. The second data set is Jingkun Highway in western-Xi'an-Area that is provided by our laboratory. It is acquired by RADARSAT-2, and obtained from a subset of a C-band single-look PolSAR image. It size is 512 × 512.

To show the advantage of our framework, the tradi-

tional SAE and SVM classifier which are based on pixels are used for comparisons[17, 21]. Then, two region-based methods: the SSAE with local spatial information (SSAEL)[16] and Wishart-based Markov random fields (WMRF)[18] are also used for comparisons. In addition, a middle step, which combines the SAE and WMRF without error correction is used to explain the effectiveness of error correction.

3.1 Experimental on Flevoland image

Figures 4(a) and (b) show the corresponding Pauli RGB image of Flevoland and the ground truth respectively. There are 6 classes in this scene include bare soil, potatoes, beet, pea, wheat and barley. In our experiments, we choose 10% samples randomly for each class for training and remaining 90% for testing.

In the experiments, there are three hidden layers and one output layer in SAE and we set the numbers of units within three hidden layers as 300. The number of iterations is set to 400. SVM parameters are adapted by five-fold cross validation. The regularization parameter in the SVM is tuned in the range of $\{10^{-2}, 10^{-1}, \cdots, 10^{3}\}$. For SSAEL, the window size is set as 5×5, and the network structure is set the same as SAE. The Wishart MRF is a region-based classifier where the window size is chosen as 5×5 for segmenting. In the experiment of SABM, the threshold value is set to 0.003 when error correction startup.

Results of comparing methods and the proposed methods are shown in Figs. 4(c)-(h). We can see that, our method is better than the other ones in the visual effect. Figure 4(c) shows the classification result with traditional SAE. It can be observed that, the classification map shows the relatively clearer boundary. As a classical algorithm for pixel-based classification, SAE performs well. As showed in the bottom red rectangle in Fig. 4(c), some pixels are misclassified and the region is not smooth enough. Figure 4(d) is the classification result of SVM. SVM perform poorly in this data. It cannot recognize pea and wheat from each other very well which is displayed in the black rectangle. Figure 4(e) is the result of SSAEL. It achieves better results than SAE and SVM. However, there are many pixels misclassified in the red rectangle. The result of WMRF is illustrated in Fig. 4(f). This method utilized the region information, so the area of the classification result is relatively smooth. On the contrary, the boundary of the classification map is not clear enough. Figure 4(g) is the proposed method without error correction. We record this method as SAE + WMRF. However, there are some pixels misclassified as showed in the black ellipses. Figure 4(h) shows the result of SABM which is utilized to clean the result of Fig. 4(g). Due to the application of pixel and region information, the classification performance is highly improved. Under the guidance of the confusion matrix, some incorrect results are corrected. For instance, bare soil cannot be identified as pea under this strategy. The result of error correction is shown in the black ellipse in Figs. 4(g) and (h). The accurate boundary and homogenous region are obtained which are clearly illustrated by red and the black rectangles in Fig. 4(h).

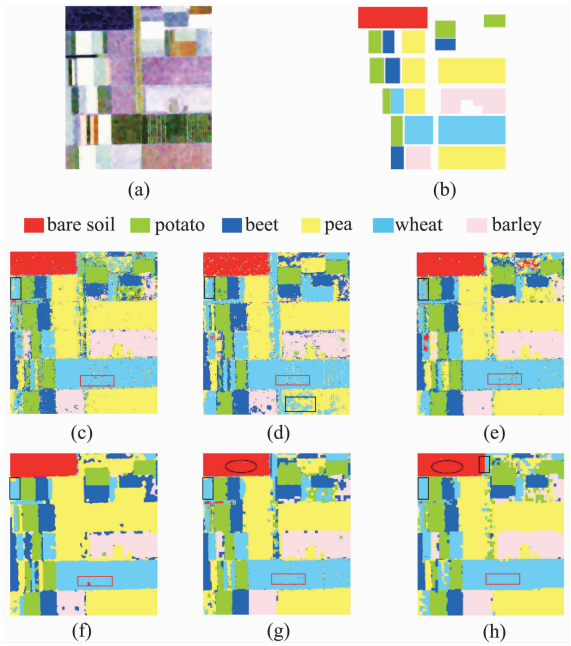

Fig. 4　(a) the PolSAR image (PauliRGB) of Flevoland, (b) The ground truth Map, (c) SAE method, (d) SVM method, (e) SSAEL method, (f) WMRF method, (g) SAE + WMRF method, (h) SABM method

图 4　(a)极化 SAR 图像 Pauli RGB 合成图, (b) 地面真值图, (c) SAE 算法, (d) SVM 算法, (e) SSAEL 算法, (f) WMRF 算法, (g) SAE + WMRF 算法, (h) 本文 SABM 算法

In the PolSAR image, there are some regions with complex terrain. In this way, these regions cannot be assigned to a certain label. Hence, there are some white areas in the ground truth map of Fig. 4(b). However, the white areas are classified to the same class with these methods. Plainly, the homogeneous region of the proposed method is smoother than the other methods in the left black rectangles.

Table 1　Classification Performance of Flevoland with Different Methods

表 1　不同算法对 Flevoland 数据的分类性能

Flevoland	bare soil	potato	beet	pea	wheat	barley	OA	Kappa
SAE	0.9747	0.8956	0.8571	0.9774	0.9511	0.9459	0.9471	0.9330
SVM	0.9354	0.8713	0.8954	0.8717	0.9478	0.8747	0.8968	0.8648
SSAEL	0.9816	0.9432	0.9318	0.9895	0.9657	0.9706	0.9703	0.9633
WMRF	0.9828	0.9304	0.9015	0.9853	0.9654	0.9407	0.9610	0.9505
SAE + WMRF	0.9838	0.9538	0.9108	0.9873	0.9725	0.9723	0.9713	0.9650
SPWMRF	0.9994	0.9750	0.8914	0.9813	0.9881	0.9762	0.9760	0.9687

We record the classification performance in Table 1. The overall accuracy (OA) is used to evaluate the performance of different methods. Accuracy is calculated by Eq. 13:

$$A = \frac{N_t}{N_g} \quad , \quad (13)$$

where A is the accuracy. For each category, N_t is the number of labeled testing pixels which are classified correctly to this class, N_g is the total number of pixels in this class in ground truth. For the total accuracy, N_t is the number of correct classifications for all the training samples and N_g is the total number of pixels in ground truth. At the same time, Kappa coefficient is computed to measure the labeling consistency of the classification result, which is recorded in Table 1. The larger the Kappa is, the better the classification performance is.

It is clearly that, for the experiment of Flevoland, the classification accuracy of SABM is the highest compared with the other methods for most classes and the best results are in bold. For the total classification accuracy, the proposed method achieved better performance. The OA is increased and the value of Kappa coefficient is the maximum. Nevertheless, not all the pixels have the true label for the whole image, so the accurate calculation is according to the pixels with the true label that is shown in Fig. 4(b).

3.2 Experimental on Xi'an-area

There are three classes of Weihe River in western-Xi'an-Area in the Fig. 5(a). They are Bench land, Urban and River. The ground truth is illustrated in Fig. 5(b). We also choose 10% samples randomly for training and the remaining 90% for testing.

For a reasonably fair comparison, in this experiment, the parameters are set to the same with the previous experiments for the comparative comparison. For the proposed method, the threshold value κ is set to 0.006 when error correction startup.

The result of classification is illustrated in Figs. 5(c)-(h). The consequence of SAE is shown in Fig. 5(c). The result indicates that the classification map of SAE is affected by the speckle noise, even though the data were filtered already. Figure 5(d) shows the classification result of SVM. Due to the reason that it is a pixel-based method, there are many scattered pixels in the figure. The result of SSAEL is shown in Fig. 5(e). As we have seen, though it classifies the river clearly. But, a lot of pixels are misclassified in the area of Urban. Figure 5(f) shows the result of WMRF. Accuracy of Urban is merely 0.6956. WMRF cannot distinguish Bench land and Urban from each other very well. Figure 5(g) indicates the result of the proposed method without error correction. It performs well in Bench land classification. However, it confuses Bench land and urban too. The classification result of SABM is shown in Fig. 5(h). Because of the application of error correction strategy, the pixels are corrected when they are classified into Bench land in the black ellipses. As a result, homogeneous region is smoother than the other method in the black ellipses. As showed in the black rectangle, the edge of the River is regular enough to compare the method without error correction strategy.

There are also some white areas in Fig. 5(b). It is clear that, the area is the most smooth for the proposed method in the right black rectangle.

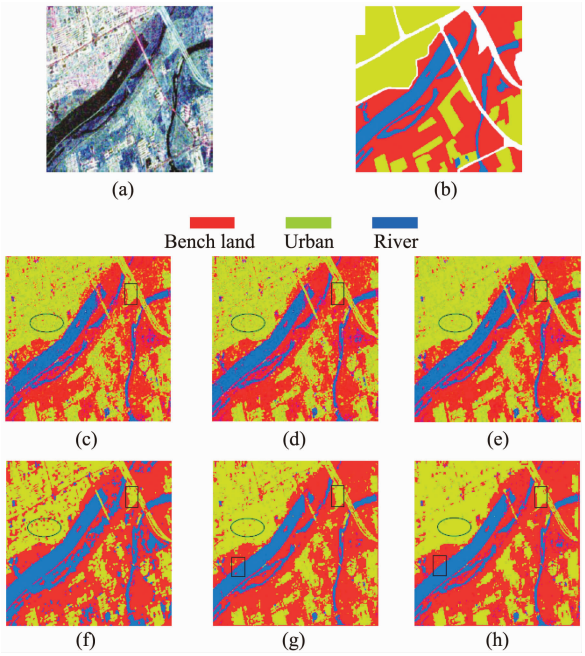

Fig. 5 (a) the PolSAR image (PauliRGB) of Xi'an-area, (b) The ground truth Map, (c) SAE method, (d) SVM method, (e) SSAEL method, (f) WMRF method, (g) SAE + WMRF method, (h) SABM method

图5 (a)极化SAR图像Pauli RGB合成图,(b)地面真值图,(c)SAE算法,(d)SVM算法,(e)SSAEL算法,(f)WMRF算法,(g)SAE + WMRF算法,(h)本文SABM算法

We list the overall accuracy and Kappa coefficient in Table 2. The (OA) is utilized to evaluate the performance of different methods which is calculated by Eq. 13. From Table 2, we can find that the total classification accuracy of the proposed method is higher than the others. The value of Kappa coefficient is greater than all other values. The remarkable results are in bold. The proposed method still offers excellent performance.

Table 2 Classification Performance of Xi'an-area with Different Methods

表2 不同算法对西安地区数据的分类性能

Weihe River	Bench land	Urban	River	OA	Kappa
SAE	0.7853	0.7968	0.8487	0.7981	0.6655
SVM	0.8523	0.7602	0.8348	0.8171	0.6915
SSAEL	0.8626	0.8095	0.8344	0.8396	0.7333
WMRF	0.7973	0.6956	0.9439	0.7834	0.6502
SAE + WMRF	0.8925	0.8179	0.8066	0.8532	0.7401
SPWMRF	0.8879	0.8392	0.8571	0.8653	0.7522

4 Conclusion

This paper proposes a new classification method applied for the PolSAR image. The method is based on SAE and BRMRF to enhance the classification accuracy

of PolSAR image. With the application of pixel and region information, we can simultaneously get the exact boundary and the coherent region of the object, simultaneously. However, an important standard to measure the classification performance is that the accurate edges and the smooth regions obtained simultaneously. There are two layers in the model. The first layer gives the initial classification of the testing sample with the SAE method and the second layer revises the probability. At the same time, boundaries got from layer1 are preserved and the error classification is corrected during the WMRF applied. The experimental results show that the method is effective for the PolSAR classification and we can get clearer classification maps compared with the other classification methods.

References

[1] Tang X, Jiao L, Emery W J. SAR image content retrieval based on fuzzy similarity and relevance feedback [J]. *IEEE Journal of Selected Topics in Applied Earth Observations & Remote Sensing*, 2017, **99**:1 - 19.

[2] Tang X, Jiao L. Fusion similarity-based reranking for SAR image retrieval [J]. *IEEE Geoscience & Remote Sensing Letters*, 2017, **14**(2):242 - 246.

[3] Ulaby F T, Elachi C. Radar polaritnetry for geoscience applications [J]. *Geocarto International*, 1990, **5**(5):38 - 38.

[4] Toan T L, Quegan S, Ferro L. Agriculture classification using POLSAR data [J]. 2005, **586**(10):32.

[5] Zribi M, Baghdadi N, Holah N, *et al*. New methodology for soil surface moisture estimation and its application to ENVISAT-ASAR multi-incidence data inversion [J]. *Remote Sensing of Environment*, 2005, **96**(3):485 - 496.

[6] Zhang S, Wang S, Jiao L C, *et al*. A novel hybrid Freeman/eigenvalue decomposition with general scattering models [J]. *Journal of Infrared & Millimeter Waves*, 2015, **34**(3):265 - 270.

[7] Lim H H, Swartz A A, Yueh H A, *et al*. Classification of Earth terrain using polarimetric synthetic aperture radar images [J]. *Journal of Geophysical Research Atmospheres*, 1989, **94**(B6):7049 - 7057.

[8] Chen C T, Chen K S, Lee J S. The use of fully polarimetric information for the fuzzy neural classification of SAR images [J]. *IEEE Transactions on Geoscience & Remote Sensing*, 2003, **41**(9):2089 - 2100.

[9] Liu F, Jiao L, Hou B, *et al*. POL-SAR image classification based on Wishart DBN and local spatial information [J]. *IEEE Transactions on Geoscience & Remote Sensing*, 2016, **54**(6):3292 - 3308.

[10] Zhang H, Shan Z, Wang C, *et al*. Polarimetric SAR image classification based on SVM classifier using Radarsat-2 Quad-Pol data[C]// *ESA Special Publication. ESA Special Publication*, 2013.

[11] Bentes C, Velotto D, Lehner S. Target classification in oceanographic SAR images with deep neural networks: Architecture and initial results [C]// *Geoscience and Remote Sensing Symposium. IEEE*, 2015:3703 - 3706.

[12] G. E. Hinton, R. Salakhutdinov. Reducing the dimensionality of data with neural networks[J]. *Science*, 2006,**313**(504): 504 - 507.

[13] Hou B, Kou H, Jiao L. Classification of Polarimetric SAR Images Using Multilayer Autoencoders and Superpixels [J]. *IEEE Journal of Selected Topics in Applied Earth Observations & Remote Sensing*, 2016, **9**(7):3072 - 3081.

[14] Wang Y, Wang G, Lan Y. PolSAR image classification based on deep convolutional neural network [J]. *Metallurgical & Mining Industry*, 2015.

[15] Xie W, Jiao L, Hou B, et al. POLSAR Image Classification via Wishart-AE Model or Wishart-CAE Model [J]. *IEEE Journal of Selected Topics in Applied Earth Observations & Remote Sensing*, 2017, PP (99):1 - 12.

[16] Zhang L, Ma W, Zhang D. Stacked Sparse Autoencoder in PolSAR Data Classification Using Local Spatial Information [J]. IEEE Geoscience & Remote Sensing Letters, 2016, **13**(9):1359 - 1363.

[17] A. Ng, "Sparse autoencoder," CS294A Lecture Notes, 2011, **72**:1 - 19.

[18] Wu Y, Ji K, Yu W, *et al*. Region-based classification of polarimetric SAR images using Wishart MRF [J]. *IEEE Geoscience & Remote Sensing Letters*, 2008, **5**(4):668 - 672.

[19] Chen C T, Chen K S, Lee J S. The use of fully polarimetric information for the fuzzy neural classification of SAR images [J]. *IEEE Transactions on Geoscience & Remote Sensing*, 2003, **41**(9):2089 - 2100.

[20] Hosseiniasl E, Zurada J M, Nasraoui O. Deep learning of part-based representation of data using sparse autoencoders with nonnegativity constraints. [J]. *IEEE Transactions on Neural Networks & Learning Systems*, 2016, **27**(12):2486 - 2498.

[21] Lardeux C, Frison P L, Tison C, *et al*. Support vector machine for multifrequency SAR polarimetric data classification[J]. *IEEE Transactions on Geoscience & Remote Sensing*, 2009, **47**(12):4143 - 4152.